New Materials for Gas Separation Applications: Mixed Matrix Membranes Made from Linear Polyimides and Porous Polymer Networks Having Lactam Groups

Carla Aguilar-Lugo[1], Fabián Suárez-García[2], Antonio Hernández[3], Jesús A. Miguel[4], Ángel E. Lozano[1,3,4], José G. de la Campa[1,], Cristina Álvarez[1,*]*

1. Instituto de Ciencia y Tecnología de Polímeros, ICTP-CSIC, Juan de la Cierva 3, E-28006 Madrid, Spain.

2. Instituto Nacional del Carbón, INCAR-CSIC, Dr. Ingeniero Francisco Pintado 26, E-33011 Oviedo, Spain.

3 SMAP, UA-UVA_CSIC, Associated Research Unit to CSIC. Universidad de Valladolid, Facultad de Ciencias, Paseo Belén 7, E-47011 Valladolid, Spain.

4. IU CINQUIMA, Universidad de Valladolid, Paseo Belén 5, E-47011 Valladolid, Spain.

ABSTRACT A set of mixed matrix membranes (MMMs) has been prepared by incorporating a triptycene-isatin porous polymer network (PPN) to three aromatic polyimides (one commercial, Matrimid, and two synthesized by us: 6FDA-6FpDA and 6FDA-TMPD) covering a wide range of performances for gas separation. The triptycene-isatin PPN is a highly microporous network having a high CO_2 uptake and high chemical and thermal stability. The good compatibility between the components (PPN content of 15 and 30% w/w) was supported by the increase in the glass transition temperature of MMMs relative to the pure polyimide membranes. The addition of the PPN particles improved the permeability of all the gases tested, by increasing diffusivity and, in some cases, gas solubility. The improvements were particularly noticeable in Matrimid-based MMMs, where gas permeability increased by 700% whilst CO_2/N_2 and CO_2/CH_4 ideal selectivities decreased by a mere 4% and 12%, respectively.

1. INTRODUCTION

The continuous and rapid increase of carbon dioxide (CO_2) emissions into the atmosphere is being driven by the current increasing demand for energy and industrialization.[1] The global warning has become a global concern as it poses a serious risk to our society due to the negative effects in the environment, the human health and the economy. The urgent need to reduce the CO_2 emissions and to lower its concentration in the atmosphere has propelled the investigation of new materials, as for instance porous solid sorbents, for carbon capture and sequestration (CCS), which provide a mid-term solution to continue using fossil energy until renewable energy technology matures.[2,3] Therefore, it is nowadays of vital importance to develop high-performance solid sorbents that allow to effectively remove the CO_2 from flue gas or from natural gas.[4] Specifically,

the solid sorbents have to be highly selective towards CO_2 over other gases, such as N_2, H_2 or CH_4, have a high CO_2 uptake capacity at low and high pressure, maintain their performance under operational conditions demanded by the industry, be easily regenerated with low energy input and, moreover, be preferably prepared from low-cost raw materials. With these premises, researchers have focused on the design and synthesis of porous solids and their potential application as CO_2 sorbents, such as metal-organic frameworks (MOFs)[5-8] and a wide variety of porous organic polymers.[9] Among the latter, covalent organic frameworks,[10] azine networks,[11-13] hyper-cross-linked polymers,[14,15] microporous organic polymers,[16,17] nanoporous azo-linked polymers,[18] benzimidazole-linked polymers,[19,20] 1,2,3-triazole linked network polymers,[21] polyphenylene network polymers,[22] and porous aromatic frameworks[23], can be mentioned.

In recent years, the addition of porous organic materials to polymer matrices has attracted a risen interest because such mixed matrix membranes (MMMs) have the potential to overcome the trade-off between gas permeability and selectivity for binary gas mixtures, which greatly limits their gas separation applications.[24,25] A thoughtful design of MMMs should combine synergistically the easy processability, good mechanical stability and low cost of polymers' matrices and the superb gas separation performance of porous fillers to simultaneously enhance gas permeability and selectivity.[26-31] However, undesirable effects such as pore blockage, polymer rigidification and, in the case of a poor polymer-filler adhesion, particle agglomeration and void formation at the interface, could appear, leading to a non-ideal behavior, and consequently to the formation of materials having bad properties.[32] The problem of incompatibility is particularly relevant in the case of inorganic fillers and consequently MMMs based on them have not been able to reach the expected performance.

Recently, we have successfully prepared a new set of porous polymer networks (PPNs) using a cost-effective and feasible methodology, which is easily scaled up to produce large quantities of material for practical applications.[33] The resulting amorphous PPNs were microporous materials, with Brunauer-Emmett-Teller (BET) surface areas varying from 580 to 790 $m^2 g^{-1}$, good chemical stability and exceptional thermal stability. They have also shown attractive properties as solid adsorbents: excellent CO_2 uptakes (up to 207 mg g^{-1} (105 cm^3(STP) g^{-1}) at 0 ºC and 1 bar) and easy regeneration by vacuum without heating (isosteric heats of CO_2 adsorption in a range between 28.3 and 35.3 kJ mol^{-1}). Moreover, under post-combustion conditions, these materials have shown selective adsorption of CO_2 over N_2 (selectivity varying from 22.5 to 32.7) comparable to those of other high-performance microporous materials.[33]

Among the PPNs prepared in the previous work, we have chosen the triptycene-isatin network as the filler to prepare MMMs because it is a highly microporous material, with a contribution of narrow micropores of about 80% of the total pore volume. The rigid, fused-ring skeleton and the three-fold symmetry (D3h) structure of the triptycene provide networks with high internal molecular free volume and high surface area.[18,19,21,34] Because of that, the triptycene-isatin network had a high CO_2 uptake (4.70 mmol g^{-1}), which could also be attributed to its favorable interaction with CO_2 through the lactam moiety.[33] The amount of CO_2 adsorbed was comparable, even superior in many cases, to the values reported for several MOFs and other regular frameworks at ambient conditions.[18,19,21,35] Thus, it would be expected that this PPN and other analogous materials would be a good alternative as fillers because they have better thermal and chemical resistance and an expectedly higher compatibility with polymer matrices than most MOFs.

In this work, three aromatic polyimides with different gas permeation properties (Matrimid® 5218, 6FDA-6FpDA and 6FDA-TMPD) have been used as polymer matrices to prepare MMMs.

Matrimid was chosen for its superior selectivity to gases, 6FDA-6FpDA for its good permeability-selectivity balance and 6FDA-TMPD for its high permeability. The MMMs were prepared with loadings of 15 and 30 % w/w, using a casting technique. The MMMs were characterized by Fourier Transform Infrared Spectroscopy, X-ray diffraction and Scanning Electron Microscopy and their thermal and mechanical properties were analyzed. Besides, the gas transport properties of the MMMs were examined to evaluate their potential application for separation of CO_2 over CH_4 and N_2.

2. EXPERIMENTAL

2.1. Materials 4,4'-(hexafluoroisopropylidene)diphthalic anhydride (6FDA) was purchased from TCI Europe and purified by sublimation at 220 ºC before use. 2,2-bis(4-aminophenyl)hexafluoropropane (6FpDA) and 2,4,6-trimethyl-*m*-phenylenediamine (TMPD) were purchased from Cymit Química and Sigma-Aldrich, respectively, and purified by sublimation at 220 ºC and 110 ºC prior to use. Matrimid® 5218 was supplied by Huntsman.

Chlorotrimethyl silane (CTMS, ≥ 99.0% of purity), anhydrous pyridine (Py, 99.8% of purity), N,N-dimethylaminopyridine (DMAP, ≥ 99.0% of purity) and acetic anhydride (99% of purity) were purchased from Sigma-Aldrich. Triptycene (98% of purity) was purchased from abcr GmbH, isatin (1H-indole-2,3-dione, 99% of purity) from Sigma-Aldrich and trifluoromethanesulfonic acid (TFSA, 99.5% of purity) from Apollo Scientific.

2.2. Synthesis of Polyimides The polyimides 6FDA-6FpDA and 6FDA-TMPD were synthesized from dianhydride 6FDA and two diamines, 6FpDA and TMPD, using an *in situ* silylation activated polyimidization method, according to the procedure reported elsewhere.[36-38]

The general synthetic procedure was as follows: a three-necked flask, equipped with a mechanical stirrer and nitrogen inlet and outlet, was charged with 5.0 mmol of diamine (6FpDA

or TMPD) and 5.0 mL of anhydrous N-methyl-2-pyrrolidone (NMP). The mixture was stirred at room temperature (RT) under a blanket of nitrogen until the diamine was completely dissolved. Then, it was cooled to 0 °C and the required amounts of CTMS (1 mol/mol reactive group, anhydrous Py (1 mol/mol reactive group) and DMAP (0.1 mol/mol Py) were added. Afterwards, the temperature was raised to RT and the solution was stirred for 10 min to ensure the formation of the silylated diamine. The solution was cooled to 0 °C again, and 5.0 mmol of 6FDA, followed by 5.0 mL of NMP, were added. The reaction mixture was allowed to reach RT, and then it was left overnight to form the poly(amic acid) solution. Following this, the poly(amic acid) was chemically imidized by adding to the solution a mixture of acetic anhydride (4 mol/mol reactive group) and Py (4 mol/mol reactive group). The solution was stirred at RT for 6 h and at 60 °C for 1 h to promote complete imidization. The polyimide solution was cooled to RT and poured into water, washed first with water and then with a mixture of water/ethanol (1/1), and finally dried in a vacuum oven at 120 °C for 6 h.

2.3. Synthesis of the Triptycene-Isatin Network PPN was obtained in quantitative yield by reacting triptycene and isatin in superacidic media according to the previously reported procedure.[33]

The preparation of the triptycene-isatin network was as follows: an oven-dried three-necked Schlenk flask, 100 mL, equipped with a mechanical stirrer and gas inlet and outlet was charged with triptycene (5.82 g, 23.0 mmol), isatin (5.07 g, 34.5 mmol) and chloroform (25 mL). The mixture was stirred at RT under a nitrogen blanket, cooled to 0 ºC and then TFSA (50 mL) was slowly added with an addition funnel for 25-30 min. The reaction mixture was allowed to warm to RT and stirred for 5 days. The product was poured into a water/ethanol mixture (3/1), filtered and consecutively washed with water, acetone and chloroform. After drying at 150 ºC for 12 h under

vacuum, the material was obtained as a tan powder in 98% yield. ^{13}C NMR (100 MHz, solid state) δ ppm 180, 145, 124, 110, 62, 55.

2.4. Film Formation Neat polymer films were prepared using a solution casting method. The general procedure was as follows: 0.50 g of polymer was dissolved in 10 mL of tetrahydrofuran (THF), and the solution was filtered through a 3.1 μm fiberglass Symta syringe filter, poured onto a glass ring placed on a leveled glass plate, covered with a watch glass, and maintained at RT overnight to remove most of the solvent. The films were peeled off from the glass and subjected to the following thermal treatment under vacuum conditions: 100 ºC for 24 h, 150 ºC for 2 h, 180 ºC for 1 h, 200 ºC for 30 min and then they were heated until 250 ºC and allowed to cool slowly.

To prepare MMMs with targeted PPN loadings (15 and 30 wt.%), the filler was previously heated at 200 ºC for 15 min, slowly cooled down to RT in a vacuum oven, and stored under vacuum before use. As an example, the preparation of MMMs containing 15 wt.% of PPN is described as follows: a suspension of filler (100.0 mg) in 10.0 mL of THF was stirred for 24 h at RT, followed by sonication for 20 min with a 130 W ultrasonic probe (Vibra Cell™ 75186) operating at 30-50% maximum amplitude. The procedure consisted in 40 cycles of 20 s ultrasonic exposures and 10 s cool-down so that the particles could be entirely dispersed. Then, 2.0 mL of a filtered polymer solution (565.0 mg of polymer in 5.0 mL of THF) was added to the suspension with stirring. The suspension was sonicated for a further 10 min (20 cycles) before adding the rest of the polymer solution and subsequently it was maintained with stirring for an additional 24 h. The films of MMMs were cast following the procedure described above.

2.5 Characterization ^{1}H and ^{13}C Nuclear Magnetic Resonance (NMR) spectra of monomers and chemicals were recorded on a Bruker Avance 400 apparatus working at 400 MHz and 100 MHz, respectively, using deuterated dimethyl sulfoxide (DMSO-*d6*) as solvent. Solid state ^{13}C

cross-polarization magic angle spinning NMR spectrum (CP-MAS ^{13}C NMR) of the porous polymer network (PPN) was recorded on a Bruker Avance 400 spectrometer equipped with a 89 mm wide bore and a 9.4 T superconducting magnet. The spectrometer operated at a Larmor frequency of 100 MHz using a contact time of 1 ms and a delay time of 3 s. The sample was spun at 9 KHz. Fourier Transform Infrared (FTIR) spectra were registered on a Perkin Elmer Spectrum RX-I FTIR spectrometer, equipped with an ATR accessory. Thermogravimetric analyses (TGA) were performed on a TA-Q500 analyzer under nitrogen flux (60 mL min^{-1}) at 10 ºC min^{-1}. The particle size distribution was determined by laser scattering using a Coulter LS320 (Beckman). Approximately 20 mg of the sample was thoroughly dispersed in 10 mL of ethanol and averages of three readings were recorded for each sample. Wide-angle-X-ray scattering (WAXS) patterns were recorded in the reflection mode at RT, using a Bruker D8 Advance diffractometer provided with a Goebel Mirror and a PSD Vantec detector. CuK_α (wavelength λ = 1.54 Å) radiation was used. A step-scanning mode was employed for the detector, with a 2θ step of 0.024º and 0.5 s per step. Scanning electron microscopy (SEM) images were taken with a QUANTA 200 FEG ESEM on Au-metallized samples operating at an acceleration voltage of 1.5 kV in high vacuum and using the detection of secondary electrons method. Density of membranes (ρ) was determined from Archimedes' principle using a top-loading electronic XS105 Dual range Mettler Toledo balance provided with a density measurement kit. The samples were sequentially weighed in air and into high purity isooctane at 25 ºC. Six density measurements were made for each sample. The density was calculated from Eq. (1):

$$\rho = \rho_{liquid}\frac{w_{air}}{w_{air} - w_{liquid}} \quad (1)$$

where ρ_{liquid} is the density of isooctane, w_{air} is the weight of the sample in air and w_{liquid} is its weight when submerged in isooctane. The fractional free volume (FFV) was estimated using the Eq. (2):

$$FFV = \frac{V - 1.3V_w}{V} \quad (2)$$

where V is the polymer specific volume and V_w is the van der Waals volume, which was calculated by molecular modeling applying the semi-empirical method Austin Model 1 (AM1) in the Hyperchem Molecular Modelling Program.[39]

Mechanical properties of membranes were evaluated under uniaxial tensile tests at RT using an MTS Synergie-200 testing machine provided with a 100 N load cell. Rectangular test pieces of 5 mm width and 25 mm length were subject to a tensile load applied at 5 mm min^{-1} until fracture. The strain was measured from cross-head separation.

2.6. Gas Transport Properties The gas permeation properties of the membranes for pure gases (He, O_2, N_2, CH_4 and CO_2) were measured at 30 °C and an upstream pressure of 3 bar using a lab-made constant volume/variable pressure apparatus. Prior to the measurement, the membrane inside the permeation cell was maintained under high vacuum overnight. Then, an upstream pressure of 3 bar was applied (t= 0 s) and the increase of the permeate pressure was recorded as a function of time. All the gases were allowed to permeate until the steady-state (ss) conditions were attained.

The gas permeability coefficients (P) were calculated from Eq. (3).

$$P = \frac{273Vl}{76ATp_0}\left[\left(\frac{dp(t)}{dt}\right)_{ss} - \left(\frac{dp(t)}{dt}\right)_{leak}\right] \quad (3)$$

where A and l are the effective area and the thickness of the membrane, respectively, V is the downstream volume, T is the absolute temperature, p_0 is the upstream pressure, $(dp(t)/dt)_{ss}$ is the steady state rate of the pressure-rise, and $(dp(t)/dt)_{leak}$ is the system leak rate, which was less than 1% of $(dp(t)/dt)_{ss}$. The diffusion coefficient (D) was determined from the relation given in Eq. (4).

$$D = \frac{l^2}{6\theta} \quad (4)$$

where θ is the time lag, corresponding to the intercept of the time axis with the straight line in the steady-state. The solubility coefficient (S) was indirectly estimated from S=P/D, assuming the validity of the solution-diffusion permeation model. Finally, the ideal selectivity for a pair of gases A and B was evaluated as the ratio of the individual gas permeabilities, which can be decoupled into diffusivity selectivity and solubility selectivity according to Eq. (5).

$$\alpha_{A/B} = \frac{P_A}{P_B} = \frac{D_A}{D_B} X \frac{S_A}{S_B} \quad (5)$$

3. RESULTS AND DISCUSSION

3.1. Characterization of PPN-Polyimide MMMs MMMs of a commercial, Matrimid® 5218, and two synthetic, 6FDA-6FpDA and 6FDA-TMPD, polyimides incorporating PPN (15 and 30 wt.% of total solid content) were prepared by dispersing freshly sonicated PPN particles in a polyimide solution, followed by film casting, as described in section 2.4. The chemical structures of the components of the MMMs are shown in Figure 1. The materials will be hereinafter referred as "name polyimide + X PPN", where X is the weight percentage of PPN.

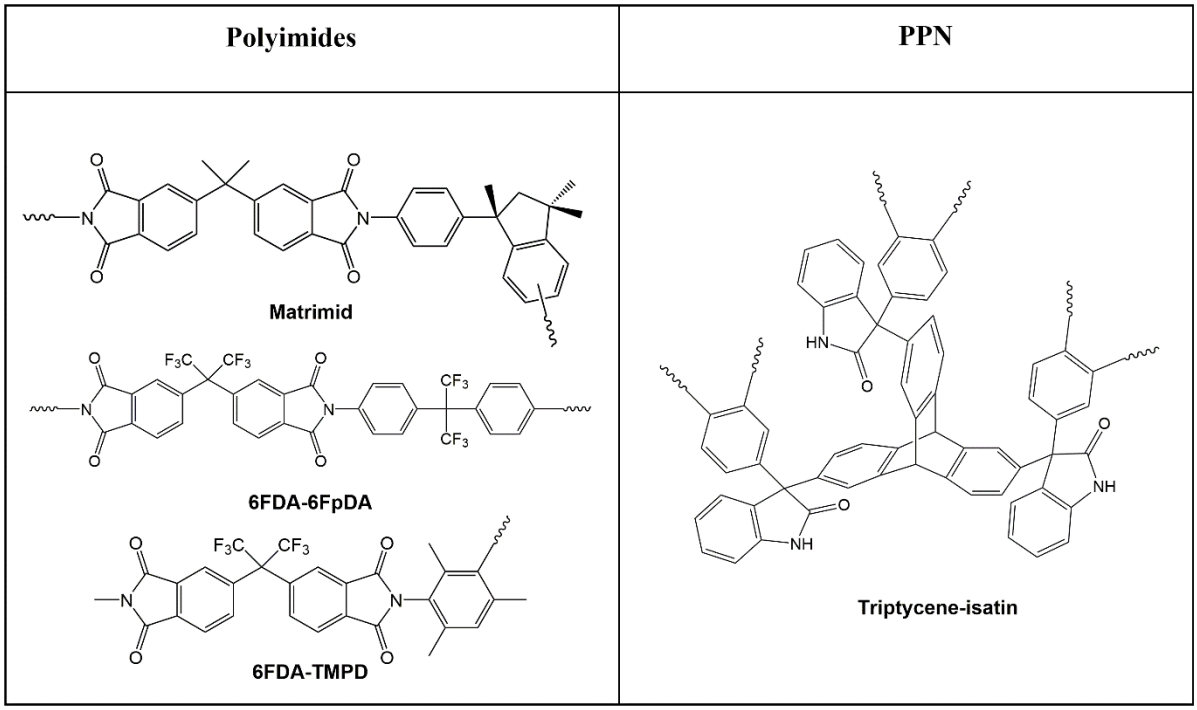

Figure 1. Chemical structures of polyimides and PPN used to prepare the MMMs.

The Coulter particle size analysis of the PPN suspension, after being stirred for 24 h and subsequently sonicated for 20 min, revealed that the highest proportion of particles corresponded to an average size of 0.39 μm. However, the bimodal size distribution of particles, which is shown in Figure 2, indicated their tendency to aggregate. Thus, in order to reduce this undesirable effect, the PPN suspension was first mixed with 40% of the polyimide solution, and sonicated for 10 min before adding the rest of the solution. This step was crucial to well mix both components, and thus to obtain a good distribution of filler in the polymeric without a visible agglomeration of the particles, even at 30 wt.% of PPN loading. All the membranes were transparent with a brown coloration, which increased with the loading, as seen in Figure 3.

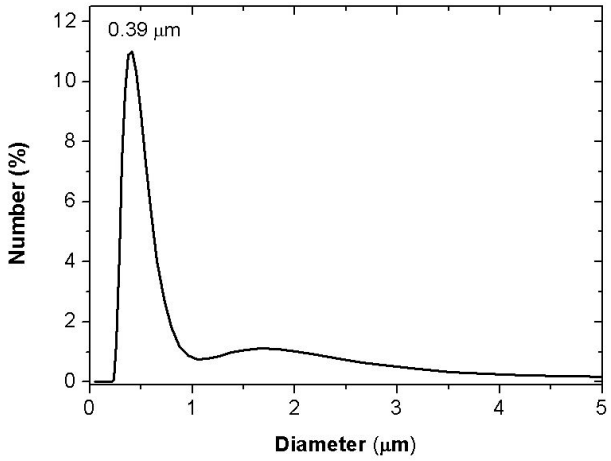

Figure 2. Particle size distribution of the porous filler suspension in ethanol after stirring for 24 h and sonicating for 20 min.

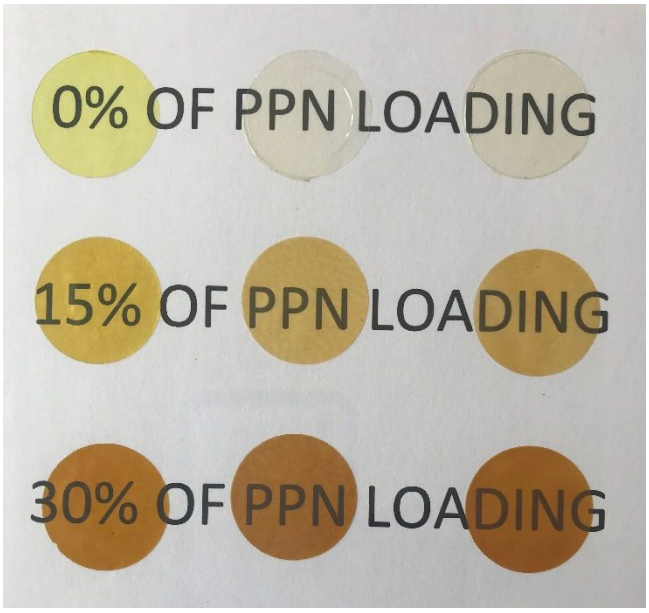

Figure 3. The physical appearance of PPN-polyimide MMMs: Matrimid (left), 6FDA-6FpDA (middle) and 6FDA-TMPD (right).

The chemical structure of the MMMs was characterized by ATR-FTIR. As an example, Figure 4 displays the spectra of the pristine PPN and polyimides, and the MMMs containing 30 wt.% of PPN loading. The FTIR spectrum of PPN displayed characteristic bands at 1708, 1470 and 1320

cm^{-1}, which were ascribed to the 5-member lactam rings coming from the isatin reaction with the aromatic compound. All the MMMs' spectra showed the typical absorption bands of imide groups at 1780 (asym C=O st), 1720 (sym C=O st), 1360 (C-N st) and 1725 cm^{-1} (imide ring deformation), which come from the polyimide matrix. Moreover, the band at 1470 cm^{-1} was also visible, confirming the presence of filler in the MMMs. Unfortunately, the other two bands associated with PPN could not to be assigned because of the overlapping with the polyimide's bands.

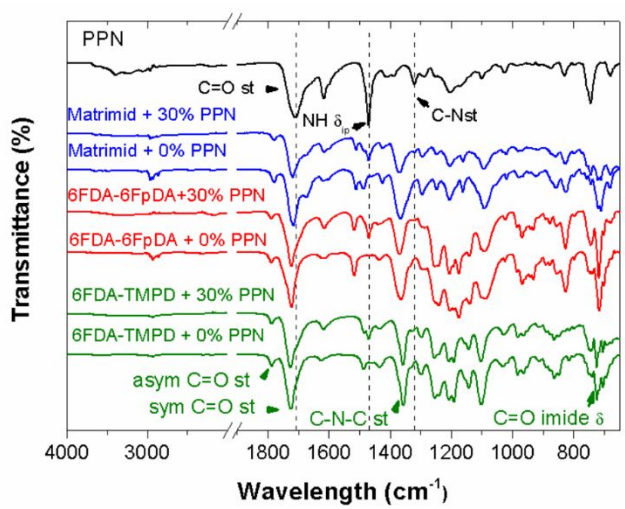

Figure 4. FTIR spectra of MMMs at 0% and 30% of PPN loading and pristine PPN.

WAXS patterns of PPN powder, pristine polyimides, and MMMs with a PPN loading of 30 wt.% are shown in Figure 5 as an example. All the systems showed the typical broad halo indicating their amorphous nature. Small changes in the shape of the amorphous halos were observed when the patterns of MMMs and pristine polyimides were compared. The position of the amorphous halo maxima of MMMs hardly varied when compared with those of their respective pristine polyimides. This maximum corresponded to the most probable intersegmental distance in the chains' packing, which was close to 0.58 nm. Moreover, the embedded filler caused changes in the packing of the polyimides, diminishing the contribution to the global scattering from the low angles side (i.e. large intersegmental distances) and increasing it from the high angles (i.e. short

intersegmental distances). This may imply changes in the FFV distribution of the membranes. The effect was more marked in the MMM derived from Matrimid, which is the polyimide with lower internal free volume.

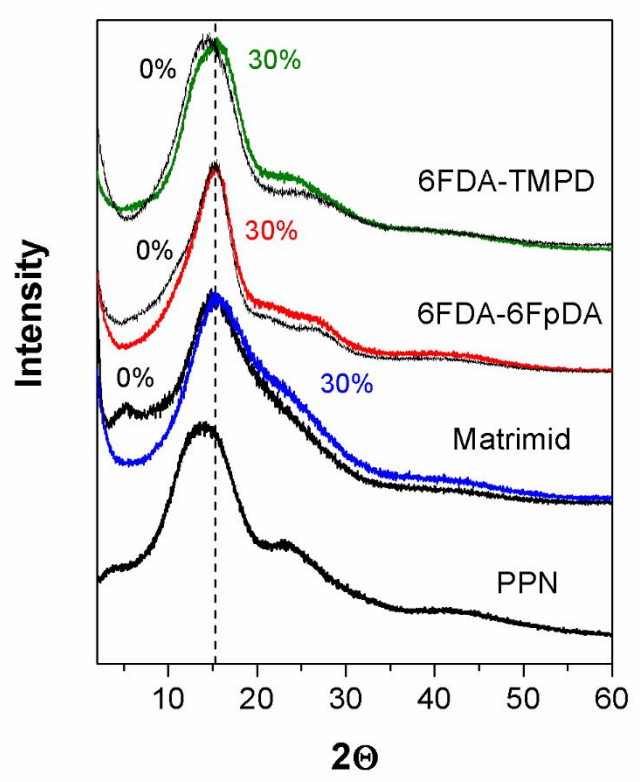

Figure 5. WAXS patterns of PPN, pristine polyimides and MMMs containing 30 wt.% of loading.

SEM images of the cross-section of the MMMs are shown in Figure 6. At 15 wt.% of loading, the compatibility of the PPN particles with all the polyimides was good, although the best compatibility was found for Matrimid. In fact, this polyimide seems to retain a good compatibility even when the PPN content increased. The visible micron-sized cavities in the SEM images could be caused by the ductile fracture mode of the membranes during the cryo-fracturing.

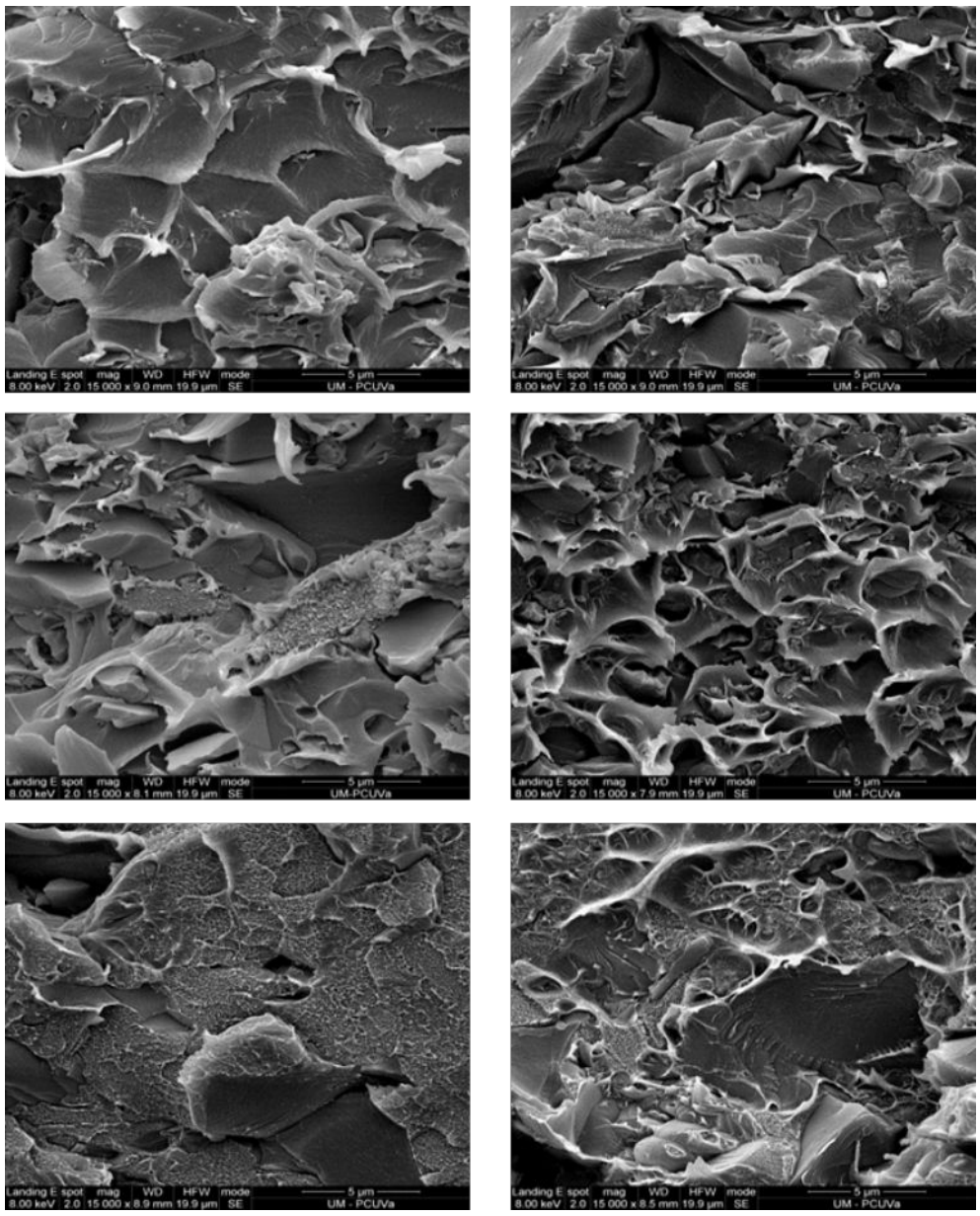

Figure 6. SEM micrographs of MMMs containing 15 (left) and 30 (right) wt.% of loading derived from Matrimid (up), 6FDA-6FpDA (middle) and 6FDA-TMPD (bottom).

3.2. Thermal Properties The glass transition temperatures, T_g, of the MMMs were determined by DSC measurements. Figure 7 shows the DSC curves of the pure polyimides, Matrimid and 6FDA-6FpDA, and their corresponding MMMs. The T_gs of the membranes derived from 6FDA-TMPD have not been shown because they were above 360 ºC, very close to the maximum

operating temperature of the DSC. The T_g of the MMMs increased with the loading content, this increment being particularly significant, about 10 ºC, in the membranes derived from Matrimid. It is known that the restriction of the molecular mobility of the polymeric chains causes an increase in its T_g.[30,40] Thus, these results indicated a favorable interaction between PPN and polyimides, which is higher for Matrimid.

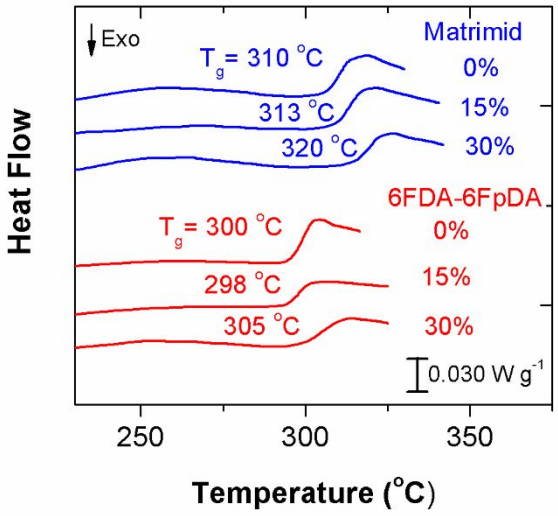

Figure 7. DSC curves of the MMMs derived from Matrimid (blue) and 6FDA-6FpDA (red).

The thermal stabilities of the MMMs were analyzed by TGA under nitrogen. Figure 8 displays the curves of weight loss and their first derivatives for the MMMs, pure polyimides and PPN. The first weight loss, below 100 ºC, in MMMs and PPN was related to the loss of humidity adsorbed in the surface of the filler. The second weight loss, between 250 and 400 ºC, of MMMs could be associated with the remaining solvent trapped in the pores (< 2 wt.%). The peak above 450 ºC in all the samples corresponded to the degradation of both the polyimide and the PPN. The onset of degradation temperature for the PPN (540 ºC) was higher than that of the polyimides (490 ºC for Matrimid, 515 ºC for 6FDA-6FpDA and 505 ºC for 6FpDA-TMPD). The high thermal stability of

the PPN led to MMMs with improved thermal stability in the case of Matrimid and similar in the other two cases. Table 1 lists physical and thermal properties of these MMMs.

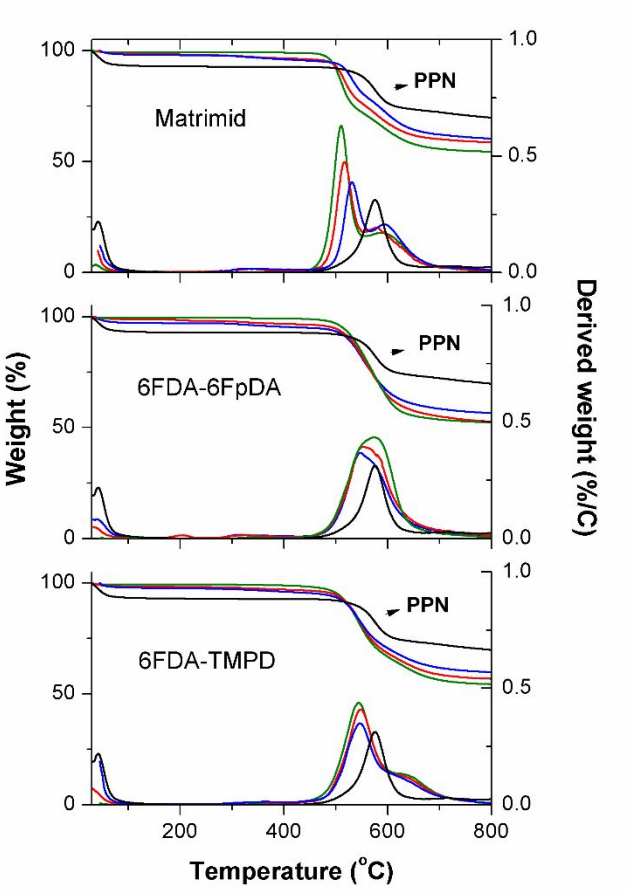

Figure 8. TGA curves of MMMs: 0 (green), 15 (red) and 30 (blue) wt.% of loading, and PPN.

Table 1. Inherent viscosity (η_{inh}), density and thermal properties

MMMs	η_{inh} (dL g^{-1})	ρ (g cm^{-3})	T_g (ºC)	T_d (ºC)[a]	R^{800} (%)[b]
Matrimid + 0% PPN	0.66	1.266	310	490	55
Matrimid + 15% PPN			313	497	61
Matrimid + 30 % PPN			320	512	63
6FDA-6FpDA + 0% PPN	0.87	1.466	300	515	52
6FDA-6FpDA + 15% PPN			298	515	54
6FDA-6FpDA + 30% PPN			305	515	59
6FDA-TMPD + 0% PPN	0.57	1.321	n.d[c]	505	54
6FDA-TMPD + 15% PPN			n.d[c]	513	59
6FDA-TMPD + 30% PPN			n.d[c]	513	62

[a)] onset of degradation temperature (T_d) of PPN was 540 ºC; [b)] char yield at 800 ºC (R^{800}) of PPN was 70%; [c)] glass transition temperature (T_g) was not detected.

3.3. Mechanical Properties

The mechanical properties of the pure polyimides and MMMs are listed in Table 2. The addition of PPN in the polyimide's matrix had a marked effect on the mechanical properties of these materials, as observed by the increase in Young's modulus and the reduction in strength and elongation at break when the loading content increased. Considering that an increment in the Young's modulus is an indicator of good interfacial adhesion between both filler and matrix, the adhesion seems to be better for Matrimid and 6FDA-6FpDA than for 6FDA-TMPD. However, the tensile strength and the elongation at break decreased. At 15 wt.% of PPN loading, the strength decreased about 55% in all the cases whereas the elongation at break decreased about 70% for Matrimid and 6FDA-6FpDA and 50% for 6FDA-TMPD. At 30 wt.% of loading, the mechanical properties decreased about 60 wt.% in strength and about 85 wt.% in elongation at break for Matrimid and 6FDA-6FpDA. The 6FDA-TMPD MMMs exhibited poor mechanical properties,

which could be related to the inferior mechanical properties of the pure 6FDA-TMPD as compared to the other two polymers. In fact, the mechanical properties of the membrane with the highest PPN content have not been reported because the elongation at break was less than 1.5%, and the standard deviations associated to the values of Young's modulus and tensile strength were very high. The embrittlement of the MMMs, despite the increase in the Young's modulus, has been observed in other MMMs,[40,41] and it is probably caused by small defects in the membranes produced either by the presence of small agglomerates or by cracking caused by the cutting of the probes.

Table 2. Mechanical properties of MMMs and pure polyimides membranes.

MMMs	Young's Modulus (GPa)	Tensile strength (MPa)	Elongation at break (ºC)
Matrimid + 0% PPN	1.28±0.07	93±3	18±3
Matrimid + 15% PPN	1.4 ± 0.1	50±5	5±1
Matrimid + 30% PPN	1.8±0.1	36±15	2±1
6FDA-6FpDA + 0% PPN	1.22±0.03	94±5	15±3
6FDA-6FpDA + 15% PPN	1.5±0.2	50±5	3.5±0.6
6FDA-6FpDA + 30% PPN	1.6±0.2	29±10	2.3±0.5
6FDA-TMPD + 0% PPN	1.6±0.1	59±5	4.7±0.2
6FDA-TMPD + 15% PPN	1.4±0.2	29±7	2.3±0.6
6FDA-TMPD + 30% PPN	---	---	---

3.4. Gas Separation Properties

Gas transport properties of the MMMs and the pure polyimides' membranes were determined for the following single gases: He, O_2, N_2, CH_4 and CO_2, at 3 bar and 30 ºC. The values of permeability, diffusivity and solubility (determined according to the solution-diffusion model)

coefficients, as well as those of ideal selectivity, diffusivity selectivity and solubility selectivity, for O_2/N_2, CO_2/N_2 and CO_2/CH_4 gas pairs, are listed in Table S1. Similar data from some triptycene-based polyimides and a polymer of intrinsic microporosity, PIM1, are also provided as additional information.

The permeability of the MMMs to the five gases increased with the PPN content, the increase being somewhat higher for the CH_4 gas. The improvement in permeability for Matrimid-based-MMMs was considerably higher than for the MMMs derived from the other two more permeable polyimides. Moreover, the selectivity for the gas pairs studied slightly decreased when the PPN loading increased. For instance, at 30 wt.% of PPN content, the O_2 permeability increased 7-fold for Matrimid, 2.5-fold for 6FDA-6FpDA and 1.5-fold for 6FDA-TMPD as compared to pure polyimide membranes, while the O_2/N_2 selectivity decreased only 1.5% for Matrimid and less than 10% in the worst case.

The addition of high FFV porous fillers in polymeric matrices should cause an increase in the gas diffusion through the pores of the filler by their internal free volume. In this case, the PPN is a highly microporous material (total pore volume: 0.44 $cm^3\ g^{-1}$), with a contribution of about 82 % of narrow pores (0.4 – 0.7 nm in diameter) and 18% of larger micropores (0.7 – 1 nm in diameter).[33] Therefore, the pore size distribution of the PPN should not limit the diffusion of the gases tested, with diameters smaller than 0.4 nm,[32] and then the diffusivity selectivity of the membranes should be close to that of the matrix, as seen in Table S1. Evidently, the formation of interfacial voids is inevitable during the membrane preparation, particularly in the solvent evaporation process, and they would contribute to generate additional free volume into the membrane, leading to an improvement in the gas diffusion. However, in our MMMs, the observed good polyimide-PPN adhesion reduced to a minimum the formation of non-selective voids.

The behaviour of MMMs was examined considering the two contributions to the permeability, namely the diffusion and solubility coefficients. Figure 9 shows graphically the variations of permeability, diffusivity and solubility coefficients of the MMMs relative to the reference polyimide membranes, as a function of both gas and PPN content. At 15 wt.% of PPN loading, the permeability increased roughly in the same proportion as the diffusivity, while the solubility coefficient remained practically constant, indicating that the increase in gas permeability was mainly due to an increase in the diffusion pathways through the membranes. At 30 wt.% of PPN loading, the diffusivity also showed the highest contribution to the permeability of the MMMs. However, in the case of the Matrimid-based MMM, the solubility contribution to the permeability turned out to be considerably higher (1.8-fold for O_2 and N_2 and 2.2-fold for CO_2 and CH_4) when compared with the MMM containing 15 wt.% of PPN. Therefore, at high loading, there was an increase of the solubility coefficient, which was particularly relevant for Matrimid.

The fractional free volume of the pure polyimide membranes (FFV), calculated from Eq. (2), using the experimental density listed in Table 1, was 0.110 for Matrimid, 0.208 for 6FDA-6FpDA and 0.218 for 6FDA-TMPD. The FFV for the PPN was estimated to be 0.352 from the skeletal density determined by He pycnometry (1.234 g cm^{-3}) and the total pore volume (0.440 cm^3 g^{-1}) measured from low-pressure N_2 adsorption isotherm. From these values, it would be expected for the addition of filler particles to cause an increase in FFV of the MMMs and this increment will depend on the polyimide used as matrix: the lower the FFV of the pure polyimide membrane, the higher the increment in FFV of the MMMs. According to this, as it can be observed in Figure 9, the increment in the diffusion coefficients for all the gases was higher for Matrimid-based MMMs than for 6FDA-based ones, as compared to the reference polyimide membranes.

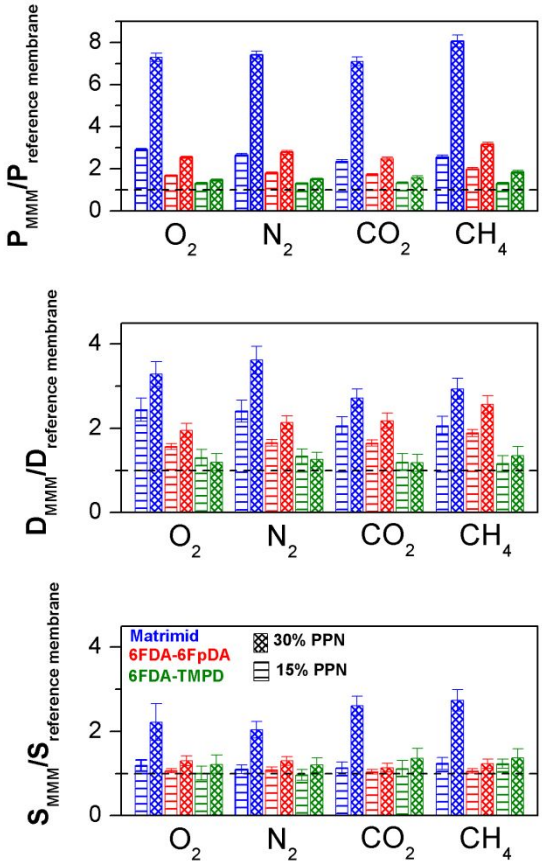

Figure 9. Changes in permeability (up), diffusivity (middle) and solubility (down) for MMMs relative to the pure polyimide membranes, which have values of 1, for every tested gas.

Clearly, the behaviour of permeability is similar to that of diffusivity (Figure 9). However, as mentioned above, the permeability increased more than the diffusivity, especially for Matrimid-based MMMs. Thus, the effect of PPN filler cannot be only limited to an increase in FFV, but also the contribution of the solubility coefficient of the filler to the gas permeability through the membrane should be considered.

We have extended the benchmarking of our MMMs via Robeson plots in Figure10, including data reported in literature for single gas permeation, corresponding to MOF-based MMMs for the separation of CO_2 from CH_4 and N_2.[42,43] Additionally, two recent benzimidazole linked polymers

(BILP)-based MMMs have been included for the separation of CO_2 from N_2.[30] All of these materials are based on Matrimid and their loading amount varied from 10 to 30 wt.%. The permeability of these MMMs was measured under conditions comparable to those used in this work (25-35 ºC and feed pressures varying between 2 and 5 bar).

The permeability mismatch between filler and matrix seems to be one of the key factors influencing the gas separation performance of our MMMs. The increase in the CO_2 permeability of the MMMs indicates that the permeability of the PPN is higher than that of the matrix. The small changes in selectivity observed for the CO_2/N_2 and CO_2/CH_4 gas pairs can be due to two possible reasons: a) the selectivity of the PPN for these gas pairs is similar or slightly lower than the selectivity of the polyimides, or b) the CO_2 permeability of the PPN is much higher than that of the polyimide matrix. In the last case, even if there is a perfect compatibility between matrix and filler, without interfacial defects, no effects on the selectivity of the MMM will be observed because there is no match on the permeability of both components, irrespective of the differences in selectivity.[44-45] Moreover, the higher the permeability differences of both components, the higher the increase in permeability of the MMM, without changes in selectivity. It is to be pointed out that the presence of the filler would cause a simultaneous increase of permeability and selectivity only if it has a high selectivity and a permeability higher than that of the matrix, but not significantly higher.

The permeability to gases of our PPN filler is unknown but, according to the comment above, it seems to have a higher permeability but a lower selectivity than all the polyimides tested. As the permeabilities of 6FDA-TMPD were about two orders of magnitude higher than those of Matrimid, the matching in permeability between matrix and filler seems to be better for 6FDA-TMPD-based MMMs. For this reason, the increase in permeability caused by the PPN filler was

significantly higher in the Matrimid-based MMMs (between 7-fold for oxygen and 8-fold for methane), without changes in selectivity. For the other two polyimides, the increase in permeability was lower (between 2.5-fold for oxygen and 3.2-fold and for methane in 6FDA-6FpDA and between 1.5-fold for oxygen and 1.85-fold for methane in 6FDA-TMPD), but there was a small decrease in selectivity because of the better permeability matching.

It should be clearly stated that the permeability increase caused by the addition of the PPN to Matrimid is higher than in all reported cases, either for fillers based on MOFs or on polymeric networks.[30,42,43] In the case of MOFs, some of the MMMs presented higher selectivities, probably because the regular structure of these MOFs assures a good homogeneity of the pores' size and provides higher size selectivity. In the case of the BILP networks, the permeability of the MMMs with higher filler content were close to our values but they were less selective. The authors indicated the formation of aggregates in these membranes at 25 wt.% of loading.[30]

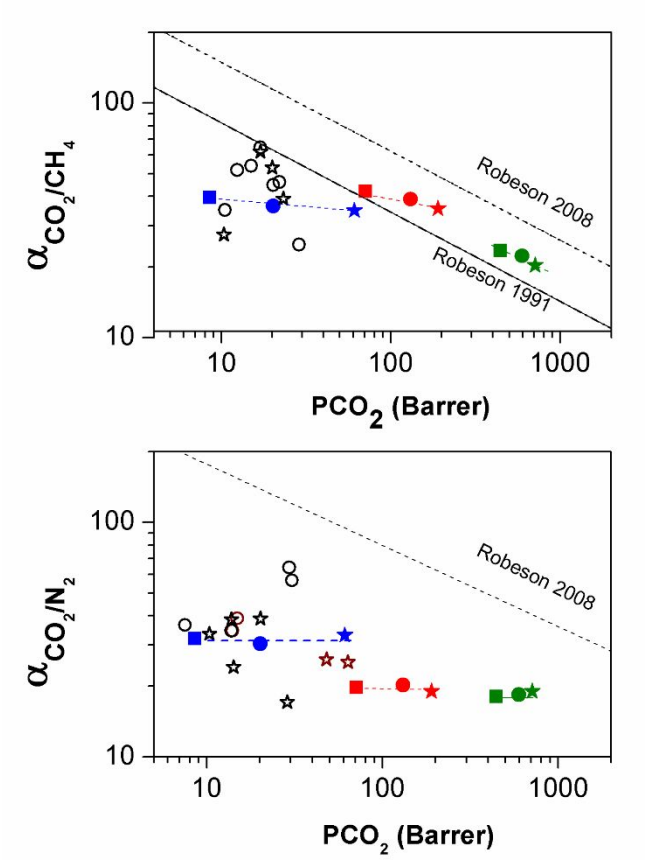

Figure 10. Upper bound limit for CO_2/CH_4 (up) and CO_2/N_2 (bottom) separation by MMMs based on Matrimid (blue), 6FDA-6F$_p$DA (red) and 6FDA-TMPD (green). The filler content in wt.% is indicated by: 0 (square), 15 (circle) and 30 (star). Open black symbols represent the experimental data reported for MOFs-based MMMs[42,43] and open wine symbols correspond to those of the polymeric network-based MMMs.[30]

4. CONCLUSIONS

A series of PPN-based MMMs has been prepared by combining linear aromatic polyimides, which cover a wide range of permeability and selectivity values (from a highly selective material as Matrimid to a highly permeable material as 6FDA-TMPD), and different load content (15 and 30 wt.%) of a highly microporous network (triptycene-isatin PPN), having high FFV (0.352) and CO_2 uptake (4.70 mmol g^{-1} at 0 ºC and 1 bar). The good compatibility shown between both

components, polyimide and PPN, provided membranes with a uniform and homogeneous dispersion of PPN particles, without interfacial voids, even for a high loading, and with good enough mechanical properties to be tested as gas separation membranes.

In general, the MMMs exhibited a significant increase in permeability, relative to the pure polyimide membranes, when the content of PPN increased, while the selectivity for gas pairs, such as O_2/N_2, CO_2/N_2 and CO_2/CH_4, was similar to that of the polyimides. Moreover, the increase in permeability of the MMM was inversely proportional to the permeability of the pure polyimide membrane. As a result of that, the combination of the less permeable polyimide, Matrimid, and the 30 wt.% of polymeric network provided membranes with excellent productivity (permeability/selectivity balance), very similar to that of 6FDA-6FpDA for CO_2/CH_4 but clearly better for CO_2/N_2, at a much lower cost.

Therefore, it can be concluded that this highly microporous material, having good compatibility with polyimides, superior chemical and thermal resistance, and high gas permeability, could be a good candidate for the separation of CO_2 over N_2 and CH_4. Despite this material is not as selective as MOFs, the choice of a highly selective polyimide as matrix will provide MMMs with much higher permeability and similar selectivity than the polymer, thus approaching the upper bound for the performance of membranes.

ASSOCIATED CONTENT

Supporting Information

Gas separation properties at 3 bar and 30 ºC of MMMs studied and some triptycene-based polyimides and PIM1 reported in the literature.

AUTHOR INFORMATION

Corresponding Author

* E.mail: jcampa@ictp.csic.es and cristina.alvarez@ictp.csic.es.

Author Contributions

The research work was made through contributions of all authors. The manuscript was written through contributions of Cristina Álvarez, José G. de la Campa, and Ángel E. Lozano.

ORCID

Carla Aguilar-Lugo: 0000-0003-4700-1564

Fabián Suárez-García: 0000-0002-1970-293X

Jesús A. Miguel: 0000-0003-2814-5941

Antonio Hernández: 0000-0002-2475-5681

Ángel E. Lozano: 0000-0003-4209-3842

José G. de la Campa: 0000-0003-1882-3104

Cristina Álvarez: 0000-0002-5000-0776

Funding Sources

This work was supported by Spain's MINECO (Projects MAT2016-76413-C2-R2, MAT2016-76413-C2-R1, MAT2015-69844-R and CTQ2016-80913-P), and the Spanish Junta de Castilla y León (Projects VA248U13 and VA051P17).

Notes

The authors declare no competing financial interest.

ACKNOWLEDGMENT

The authors would like to gratefully acknowledge Dr. Manuel Avella-Romero for the SEM images taken at the SEM-TEM Microscopy Facilities of the University of Valladolid; and Judit González Jarillo for the characterization of the mixed matrix membranes and the gas separation measurements.

REFERENCES

(1) Edenhofer, O.; Pichs-Madruga, R.; Sokona, Y.; Minx, J. C.; Farahani, E.; Susanne, K.; Seyboth, K.; Adler, A.; Baum, I.; Brunner, S.; Eickemeier, P.; Kriemann, B.; Savolainen, J.; Schlomer, S.; von Stechow, C.; Zwickel, T. Working Group III Contribution to the Fifth Assessment Report of the Intergovernmental Panel on Climate Change, Climate Change 2014: Mitigation of Climate Change; Cambridge University Press, 2015.

(2) Glier, J. C.; Rubin, E. S. Assessment of Solid Sorbents as a Competitive Post-Combustion CO_2 Capture Technology. *Energy Procedia*. **2013**, *37* (2013) 65-72.

(3) Bui, M.; Adjiman, C. S.; Bardow, A.; Anthony, E. J.; Boston, A.; Brown, S.; Fennell, P. S.; Fuss, S.; Galindo, A.; Hackett, L. A.; Hallett, J. P.; Herzog, H. J.; Jackson, G.; Kemper, J.; Krevor, S.; Maitland, G. C.; Matuszewski, M.; Metcalfe, I. S.; Petit, C.; Puxty, G.; Reimer, J.; Reiner, D. M.; Rubin, E. S.; Scott, S. A.; Shah, N.; Smit, B.; Martin Trusler, J. P.; Webley, P.; Wilcox, J.; MacDowell, N. Carbon Capture and Storage (CCS): the Way Fordward. *Energy Environ. Sci.* **2018**, *11*, 1062-1176.

(4) Lee, S. -Y.; Park, S. -J. A Review on Solid Adsorbents for Dioxide Capture. *J. Ind. Eng. Chem.* **2015**, *23*, 1-11.

(5) Bae, Y. -S.; Snurr, R. Q. Development and Evaluation of Porous Materials for Carbon Dioxide Separation and Capture. *Angew. Chem. Int. Ed.* **2011**, *50*, 11586-11596.

(6) Liu, J.; Thallapally, P. K.; McGrail, B. P.; Brown, D. R.; Liu, J. Progress in Adsorption-Based CO_2 Capture by Metal-Organic Frameworks. *Chem. Soc. Rev.* **2012**, *41*, 2308-2322.

(7) Li, J. -R.; Sculley, J.; Zhou, H. -C. Metal-Organic Frameworks for Separations. *Chem. Rev.* **2012**, *112*, 869-932.

(8) Furukawa, H.; Cordova, K. E.; O'Keeffe, M.; Yaghi, O. M. The Chemistry and Applications of Metal-Organic Frameworks. *Science.* **2013**, *341*, 123044.

(9) Das, S.; Heasman, P.; Ben, T.; Qiu, S. Porous Organic Materials: Strategic Design and Structure−Function Correlation. *Chem. Rev.* **2017**, *117*, 1515-1563.

(10) Côte, A. P.; Benin, A. I.; Ockwig, N. W.; O′Keeffe, M.; Matzger, A. J.; Yaghi, O. M. Porous, Crystalline, Covalent Organic Frameworks. *Science.* **2005**, *310*, 1166-1170.

(11) Puthiaraj, P.; Kim, S. -S.; Ahn, W. -S. Covalent Triazine Polymers Using a Cyanuric Chloride Precursor via Friedel–Crafts Reaction for CO2 Adsorption/Separation. *Chem. Eng. J.* **2016,** *283*, 184-192.

(12) Wang, K.; Huang, H.; Liu, D.; Wang, C.; Li, J.; Zhong, C. Covalent Triazine-Based Frameworks with Ultramicropores and High Nitrogen Contents for Highly Selective CO_2 Capture. *Environ. Sci. Technol.* **2016**, *50*, 4869-4876.

(13) Dang, Q. -Q.; Zhan, Y. -F.; Wang, X. -M.; Zhang, X.-M. Heptazine-Based Porous Framework for Selective CO2 Sorption and Organocatalytic Performances. *ACS Appl. Mater. Interfaces.* **2015**, *7*, 28452-28458.

(14) Saleh, M.; Lee, H. M.; Kemp, K. C.; Kim, K. S. Highly Stable CO_2/N_2 and CO_2 /CH_4 Selectivity in Hyper-Cross-Linked Heterocyclic Porous Polymers. *ACS Appl. Mater. Interfaces*. **2014**, *6*, 7325-7333.

(15) Puthiaraj, P.; Ahn, W. -S. CO_2 Capture by Porous Hyper-Cross-Linked Aromatic Polymers Synthesized Using Tetrahedral Precursors. *Ind. Eng. Chem. Res.* **2016**, *55*, 7917-7923.

(16) Dawson, R.; Stöckel, E.; Holst, J. R.; Adams, D. J.; Cooper, A .I. Microporous Organic Polymers for Carbon Dioxide Capture. *Energy Environ. Sci.* **2011**, *4*, 4239-4245.

(17) Preis, E.; Widling, C.; Scherf, U.; Patil, S.; Brunklaus, G.; Schmidt, J.; Thomas, A. Aromatic, Microporous Polymer Networks with High Surface Area Generated in Friedel–Crafts-Type Polycondensations. *Polym. Chem.* **2011**, *2*, 2186-2189.

(18) Arab, P.; Rabbani, M. G.; Sekizkardes, A. K.; İslamoğlu, T.; El-Kaderi, H. M. Copper (I)-Catalyzed Synthesis of Nanoporous Azo-Linked Polymers: Impact of Textural Properties on Gas Storage and Selective Carbon Dioxide Capture. *Chem. Mater.* **2014**, *26*, 1385-1392.

(19) Rabbani, M. G.; El-Kaderi, H. M. Synthesis and Characterization of Porous Benzimidazole-Linked Polymers and their Performance in Small Gas Storage and Selective Uptake. *Chem. Mater.* **2012**, *24*, 1511-1517.

(20) Sekizkardes, A. K.; Altarawneh, S.; Kahveci, Z.; İslamoğlu, T.; El-Kaderi, H. M. Highly Selective CO_2 Capture by Triazine-Based Benzimidazole-Linked Polymers. *Macromolecules.* **2014**, *47*, 8328-8334.

(21) Mondal, S.; Das, N. Triptycene Based 1,2,3-Triazole Linked Network Polymers (TNPs): Small Gas Storage and Selective CO_2 Capture. *J. Mater. Chem. A.* **2015**, *3*, 23577-23586.

(22) Msayib, K. J.; McKeown, N. B. Inexpensive Polyphenylene Network Polymers with Enhanced Microporosity. *J. Mater. Chem.* A. **2016**, *4*, 10110-10113.

(23) Li, L.; Ren, H.; Yuan, Y.; Yu, G.; Zhu, G. Construction and Adsorption Properties of Porous Aromatic Frameworks via $AlCl_3$-Triggered Coupling Polymerization. *J. Mater. Chem. A.* **2014**, *2*, 11091-11098.

(24) Dechnik, J.; Gascon, J.; Doonan, C. J.; Janiak, C.; Sumby, C. J. Mixed-Matrix Membranes. *Angew. Chem. Int. Ed.* **2017**, *56*, 9292-9310.

(25) Galizia, M.; Chi, W. S.; Smith, Z. P.; Merkel, T. C.; Baker, R. W.; Freeman, B. D. 50th Anniversary Perspective: Polymers and Mixed Matrix Membranes for Gas and Vapor Separation: a Review and Prospective Opportunities. *Macromolecules.* **2017**, *50*, 7809-7843.

(26) Kang, Z.; Peng, Y.; Qian, Y.; Yuan, D.; Addicoat, M. A.; Heine, T.; Hu, Z.; Tee, L.; Guo, Z; Zhao, D. Mixed Matrix Membranes (MMMs) Comprising Exfoliated 2D Covalent Organic Frameworks (COFs) for Efficient CO2 Separation. *Chem. Mater.* **2016**, *28*, 1277-1285.

(27) Mitra, T.; Bhavsar, R. S.; Adams, D. J.; Budd, P. M.; Cooper, A. I. PIM-1 Mixed Matrix Membranes for Gas Separations Using Cost-Effective Hypercrosslinked Nanoparticle Fillers. *Chem. Commun.* **2016,** *52*, 5581-5584.

(28) Jusoh, N.; Yeong, Y. F.; Lau, K. K.; Shariff, A. M. Enhanced Gas Separation Performance Using Mixed Matrix Membranes Containing Zeolite T and 6FDA-Durene Polyimide. *J. Membr. Sci.* **2017**, *525*, 175-186.

(29) Shan, M.; Seoane, B.; Andres-Garcia, E.; Kapteijn, F.; Gascon, J. Mixed-Matrix Membranes Containing an Azine-Linked Covalent Organic Framework: Influence of the Polymeric Matrix on Post-Combustion CO_2-Capture. *J. Membr. Sci.* **2018**, *549*, 377-384.

(30) Tessema, T. D. M.; Venna, S. R.; Dahe, G.; Hopkinson, D. P.; El-Kaderi, H. M.; Sekizkardes, A. K. Incorporation of Benzimidazole Linked Polymers into Matrimid to Yield Mixed Matrix Membranes with Enhanced CO_2/N_2 Selectivity. *J. Membr. Sci.* **2018**, *554*, 90-96.

(31) Shan, M.; Seoane, B.; Pustovarenko, A.; Wang, X.; Liu, X.; Yarulina, I.; Abou-Hamad, E.; Kapteijn, F.; Gascon, J. Benzimidazole Linked Polymers (BILPs) in Mixed-Matrix Membranes: Influence of Filler Porosity on the CO_2/N_2 Separation Performance. *J. Membr. Sci.* **2018**, *566*, 213-222.

(32) Moore, T. T.; Koros, W. J. Non-Ideal Effects in Organic–Inorganic Materials for Gas Separation Membranes. *J. mol. Struc.* **2005**, *739*, 87-98.

(33) Lopez-Iglesias, B.; Suárez-García, F.; Aguilar-Lugo, C.; González Ortega, A.; Bartolomé, C.; Martínez-Ilarduya, J. M.; de la Campa, J.G.; Lozano, A.E.; Alvarez, C. Microporous Polymer Networks for Carbon Capture Applications. *ACS Appl. Mater. Interfaces.* **2018**, *10*, 26195-26205.

(34) Zhang, C.; Liu, Y.; Li, B.; Tan, B.; Chen, C. -F.; Xu, H. –B.; Yang, X. –L. Triptycene-Based Microporous Polymers: Synthesis and their Gas Storage Properties. *ACS Macro Lett.* **2012**, *1*, 190-193.

(35) Keskin, S.; van Heest, T. M; Sholl, D. S. Can Metal–Organic Framework Materials Play a Useful Role in Large-Scale Carbon Dioxide Separations? *ChemSusChem.* **2010**, *3*, 879-891.

(36) Muñoz, D. M.; de la Campa, J. G.; de Abajo, J.; Lozano, A. E. Experimental and Theoretical Study of an Improved Activated Polycondensation Method for Aromatic Polyimides. *Macromolecules.* **2007**, *40*, 8225-8232.

(37) Muñoz, D. M.; Lozano, A. E.; de la Campa, J. G.; de Abajo, J. Monomer Reactivity and Steric Factors Affecting the Synthesis of Aromatic Polyamides. *High Perform. Polym.* **2007**, *19*, 592-602.

(38) Muñoz, D. M.; Calle, M.; de la Campa, J. G.; de Abajo, J.; Lozano, A. E. An Improved Method for Preparing Very High Molecular Weight Polyimides. *Macromolecules.* **2009**, *42*, 5892-5894.

(39) HyperChem(TM) Professional, Hypercube, Inc. (Version 8.0.3), Florida, USA.

(40) Chen, K.; Xiang, L.; Dong, X.; Han, Y.; Wang, C.; Sun, L. –B.; Pan, Y. Enhanced CO_2/CH_4 Separation Performance of Mixed-Matrix Membranes trough Dispersion of Sorption-Selective MOF Nanocrystals. *J. Membr. Sci.* **2018**, *563*, 360-370.

(41) Mahdi, E. M.; Tan, J.-C. Mixed-Matrix Membranes of Zeolitic Imidazolate Framework (ZIF-8)/Matrimid Nanocomposite: Thermo-Mechanical Stability and Viscoelasticity Underpinning Membrane Separation Performance. *J. Membr. Sci.* **2016**, *498*, 276-290.

(42) Seoane, B.; Coronas, J.; Gascon, I.; Etxeberria-Benavides, M.; Karvan, O.; Caro, J.; Kapteijn, F.; Gascon, J. Metal Organic Framework Based Mixed Matrix Membranes: a Solution for Highly Efficient CO_2 Capture?. *Chem. Soc. Rev.* **2015**, *44*, 2421-2454.

(43) Bae, T. -H.; Lee, J. S.; Qiu, W.; Koros, W. J.; Jones, C. W.; Nair, S. High-Performance Gas-Separation Membrane Containing Submicrometer-Sized Metal–Organic Framework Crystals. *Angew. Chem. Int. Ed.* **2010**, *49*, 9863-9866.

(44) Zimmerman, C. M.; Singh, A.; Koros, W. J. Tailoring Mixed Matrix Composite Membranes for Gas Separations. *J. Membr. Sci.* **1997**, *137*, 145-154.

(45) Keskin, S.; Sholl, D. S. Selecting Metal Organic Frameworks as Enabling Materials in Mixed Matrix Membranes for High Efficiency Natural Gas Purification. *Energy Environ. Sci.* **2010**, *3*, 343-351.

TOC GRAPHIC

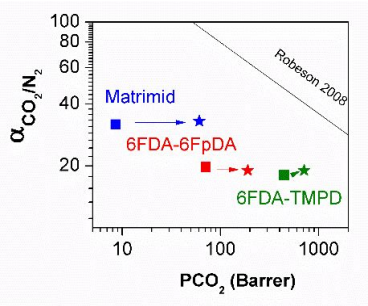

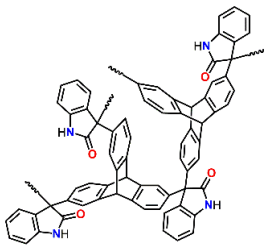

MMMs (30 wt.% of PPN content)